

Available online at [www.sciencedirect.com](http://www.sciencedirect.com)

SciVerse ScienceDirect

journal homepage: [www.elsevier.com/locate/ijhydene](http://www.elsevier.com/locate/ijhydene)

# Evaluation of the oxidation and Cr evaporation properties of selected FeCr alloys used as SOFC interconnects

Rakshith Sachitanand\*, Mohammad Sattari, Jan-Erik Svensson, Jan Froitzheim

The High Temperature Corrosion Centre, Chalmers University of Technology, 41296 Gothenburg, Sweden

## ARTICLE INFO

### Article history:

Received 18 June 2013

Received in revised form

19 August 2013

Accepted 11 September 2013

Available online 5 October 2013

### Keywords:

SOFC

Interconnect

Corrosion

Cr evaporation

Steel

## ABSTRACT

In recent years, a number of ferritic interconnect materials for use in solid oxide fuel cells (SOFC) have been developed and are now commercially available. Although similar, there are substantial variations in minor alloying elements. This study compares the oxidation performance of five such interconnect materials: Crofer 22 H, Crofer 22 APU (ThyssenKrupp VDM), Sanergy HT (Sandvik Materials Technology), ZMG232 G10 (Hitachi Metals) and E-Brite (ATI Allegheny Ludlum).

1000 h exposures have been carried out in tubular furnaces at 850 °C, with 6 l/min airflow and 3% H<sub>2</sub>O to simulate the air side atmosphere in an SOFC. In addition to the oxidation tests, time resolved in-situ chromium evaporation measurements have been carried out using a novel denuder technique. It was found that higher Mn concentrations in the alloy lead to lower Cr evaporation. Nonetheless, all steels exhibit substantial Cr volatilization and coatings are needed for most SOFC applications. Furthermore, this study demonstrates that the mass gain data alone can be misleading, and the mass loss due to Cr volatilization needs to be taken into account. Neglecting Cr evaporation results in an underestimation of the oxidation rate by between 15% and 200% for the studied steel grades.

Copyright © 2013, The Authors. Published by Elsevier Ltd. Open access under [CC BY-NC-ND license](http://creativecommons.org/licenses/by-nc-nd/3.0/).

## 1. Introduction

With the existing trend towards lower operating temperatures for solid oxide fuel cells (SOFC) metallic materials are now favoured over ceramics as construction materials for interconnects [1]. With the exception of Cr-based materials produced by Plansee, ferritic steels have become the material of choice for interconnect plates in SOFCs due to their low area specific resistance (ASR), good fabricability, suitable

mechanical properties and thermal expansion compatibility with other SOFC components. A number of commercial ferritic stainless steels are available today that have been specifically designed for SOFC applications. While they have largely similar compositions, these alloys differ from one another with respect to the quantity and type of minor alloying elements.

All of these materials form a protective Cr<sub>2</sub>O<sub>3</sub> surface scale that provides a good compromise between corrosion

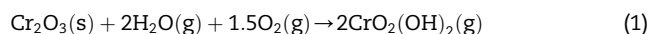
\* Corresponding author. Tel.: +46 772 2887; fax: +46 772 2853.

E-mail address: [rakshith@chalmers.se](mailto:rakshith@chalmers.se) (R. Sachitanand).

0360-3199 Copyright © 2013, The Authors. Published by Elsevier Ltd. Open access under [CC BY-NC-ND license](http://creativecommons.org/licenses/by-nc-nd/3.0/).

<http://dx.doi.org/10.1016/j.ijhydene.2013.09.044>

protection and electronic conductivity. A critical issue with chromia based oxide scales is the evaporation of Cr from the oxide–gas interface. The evaporated Cr that leaves the surface eventually deposits onto and poisons the cathode, leading to significant performance degradation [2]. The predominant volatile species of Cr are  $\text{CrO}_3$  and  $\text{CrO}_2(\text{OH})_2$  [3]. The latter requires the presence of  $\text{H}_2\text{O}$  to form (see Equation (1)) and is for most practical applications the dominant volatile compound. While much research has focussed on the effects of cathode poisoning [4,5], few groups have managed to accurately quantify the evaporation of Cr from the interconnect in a time resolved manner.



Most ferritic steels used in SOFC applications are alloyed with Mn, which results in the formation of a Mn-spinel cap layer on top of the Cr-oxide during oxidation. The result is a significant reduction in Cr evaporation [6,7]. This is still too high for SOFC applications [8] which prompts the use of barrier coatings to further suppress the evaporation rate, e.g. [6,7,9–15].

Ferritic steels for interconnect applications can be roughly classified into two categories: (1) low Si steels that contain no Nb; these steels are generally more expensive to manufacture and require special vacuum melting practices. (2) Steels with higher quantities of Si combined with significant additions of Nb; the addition of Nb causes the formation of Laves phase ( $\text{Fe}_2\text{Nb}$ ) precipitates that tie up the Si and thus minimize the formation of  $\text{SiO}_2$  at the metal–oxide interface [16]. A higher tolerance for Si results in lower manufacturing costs by allowing a shift to more conventional production techniques [16].

## 2. Materials and methods

Five commercial interconnect materials were selected for this comparative analysis. Their compositions (weight%) are presented in Table 1. Crofer 22 APU (ThyssenKrupp VDM) and ZMG232 G10 (Hitachi Metals) have low Si contents and the latter also has about 1 wt.% Cu for the purpose of further reducing Cr evaporation [17]. Sanergy HT [18] (Sandvik Materials Technology AB) and Crofer 22 H (ThyssenKrupp VDM) [16] are Laves phase forming alloys with Nb/Si ratios of 5.9 and 1.25 respectively while the alloy E-Brite (ATI Allegheny Ludlum) stands out for its low Mn and higher (26%) Cr content in addition to an Nb/Si ratio of 0.5. A detailed discussion of the effects of Nb, W, and Si in Fe–22Cr steels can be found e.g. in Refs. [16,19–21].

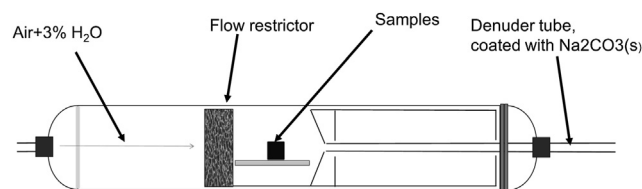


Fig. 1 – Schematic diagram of the experimental setup.

The experiments were carried out at 850 °C in a horizontal quartz tube reactor. The atmosphere consisted of air that was humidified with 3 vol%  $\text{H}_2\text{O}$  using a bubbling flask–condenser arrangement [7]. A flow rate of 6000 ml/min corresponding to an average gas velocity of 27 cm/s was selected in order to ensure a flow independent regime in the reactor [18]. A porous SiC flow restrictor was placed upstream (10 mm) of the samples in order to minimize natural convection and to obtain a more uniform flow pattern. The experimental setup is schematically represented in Fig. 1.

The chromium evaporation measurement setup consisted of a quartz denuder tube coated with  $\text{Na}_2\text{CO}_3$  which acted as the reactor outlet. The  $\text{CrO}_2(\text{OH})_2$  vapours formed during evaporation reacted with the  $\text{Na}_2\text{CO}_3$  to form  $\text{Na}_2\text{CrO}_4$  according to Equation (2):



The denuder was subsequently leached with deionized water. The Cr content in the solution was then quantified using a spectrophotometer. A more detailed description of the procedure can be found in Ref. [18].

The exposures were performed on samples in an as-received state; i.e. no surface pre-treatment was carried out prior to exposure except for a degreasing and cleaning step in acetone and ethanol using an ultrasonic bath. Gravimetric measurements were made using a six-decimal Sartorius balance. The steel sheets were cut into 15 × 15 mm square coupons. With the exception of the E-Brite sheet which was 0.5 mm (0.2”), all sheets were 0.2 mm thick. This deviation had to be taken into account in order to be able to work with as-received samples. It has been shown that the oxidation rate depends on material thickness [20,22] and is expected to be higher for a 0.2 mm thick sample than for the 0.508 mm thick sample that was used in this study.

Two types of exposures were performed. First, Cr evaporation was measured by isothermally exposing triplicates of one steel type. In this set of exposures, the denuder tubes were replaced without disturbing the experimental setup, allowing for uninterrupted measurement of Cr evaporation. Second,

Table 1 – Manufacturer supplied compositions of investigated steels specified for the received batch.

Name	Manufacturer	Thickness (mm)	Fe	Cr	Mn	Si	W/Mo	Nb	Cu	RE
E-Brite	ATI Allegheny Ludlum	0.508	Bal	26	0.08	0.2	0.87Mo	0.12	–	–
ZMG232 G10	Hitachi Metals	0.2	Bal	23.7	0.28	0.02	1.4W	–	0.93	0.07La/0.28Zr
Sanergy HT	Sandvik Materials Technology	0.2	Bal	21.2	0.3	0.12	0.96Mo	0.71	–	0.24Zr
Crofer 22 H	ThyssenKrupp VDM	0.2	Bal	22.7	0.42	0.2	1.4W	0.55	–	0.08La
Crofer 22 APU	ThyssenKrupp VDM	0.2	Bal	22.7	0.48	0.02	–	–	–	0.09La

samples from each of the investigated steels were discontinuously exposed together in the same furnace over 1000 h in order to obtain directly comparable data. The exposures were repeated thrice to ensure statistical accuracy. Selected samples were mounted in epoxy and mechanically polished to obtain cross sections. Before mounting, the samples were sputter coated with Au and subsequently coated with Ni in an electrolytic bath. The Ni layer mechanically supports the oxide scale and improves the contrast between the oxide scale and epoxy material. The samples were analysed in a LEO Ultra 55 FEG SEM equipped with an Oxford Instruments Energy Dispersive X-ray spectrometer (EDX) system. X-ray diffraction analysis (XRD) was carried out using a Siemens D5000 diffractometer setup for grazing incidence operation. A Cu-K $\alpha$  X-ray source was used with an incident angle of 5°.

### 3. Results

Fig. 2 presents discontinuous gravimetric measurements for the selected steels in air + 3% H<sub>2</sub>O at 850 °C. Crofer 22 H and Crofer 22 APU exhibited higher mass gains than the other 22% Cr steels. Crofer 22 APU had a mass gain of  $1.41 \pm 0.03$  mg/cm<sup>2</sup> while Crofer 22 H had a mass gain of  $1.24 \pm 0.03$  mg/cm<sup>2</sup> after 1000 h. Sanergy HT, a steel of similar composition to Crofer 22 H, showed a lower mass gain of  $0.89 \pm 0.07$  mg/cm<sup>2</sup> after 1000 h. The low Si, Cu containing steel ZMG232 G10 showed a mass gain of  $0.68 \pm 0.06$  mg/cm<sup>2</sup> after 1000 h. The alloy E-Brite appeared to exhibit a mass loss over time. After 1000 h, the negative mass gain was measured to be  $-0.56 \pm 0.12$  mg/cm<sup>2</sup>.

Fig. 3 presents the results of time resolved Cr evaporation measurements carried out on the investigated alloys under isothermal conditions. Crofer 22 APU exhibited the lowest evaporation ( $7.8 \times 10^{-4}$  kg/m<sup>2</sup> or 0.078 mg/cm<sup>2</sup> after 500 h) of all the alloys while that for Crofer 22 H was slightly higher. The evaporation rate for Sanergy HT was higher still, while ZMG232 G10 had a rate that was almost twice as high as for Crofer 22 APU. A significantly higher Cr evaporation rate was measured from E-Brite, a factor of four higher than for Crofer 22 APU. The measured values were in good agreement with

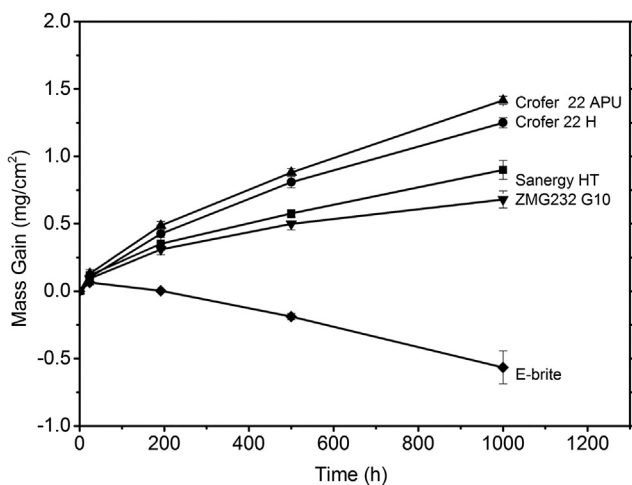


Fig. 2 – Discontinuous gravimetric measurements for the selected steels in air + 3% H<sub>2</sub>O at 850 °C.

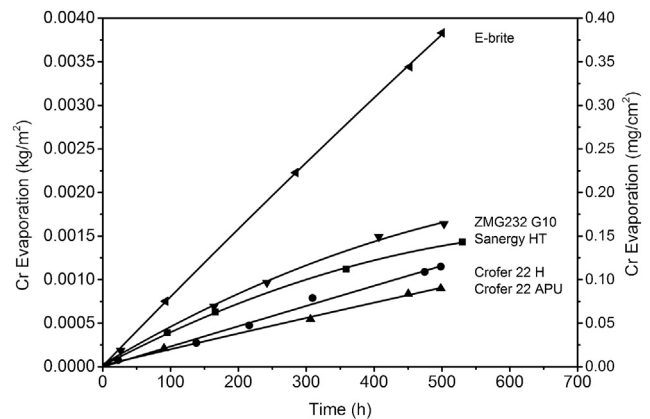
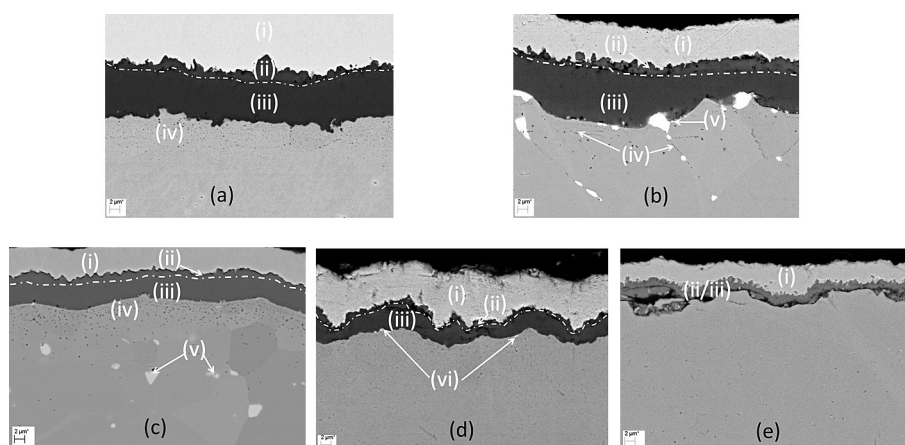


Fig. 3 – Chromium evaporation curves for the selected steels in air + 3% H<sub>2</sub>O at 850 °C.

previous Cr evaporation measurements reported in literature. Stanislawski et al. [8] have reported chromium evaporation data for the steel Crofer 22 APU at 800 °C in air + 1.8% H<sub>2</sub>O. The value reported after 500 h is approximately  $5.4 \times 10^{-4}$  kg/m<sup>2</sup>. The difference between the measured values in the present investigation ( $7.8 \times 10^{-4}$  kg/m<sup>2</sup>) and those measured by Stanislawski et al. is attributed to the lower temperature and humidity used in Ref. [8]. Casteel et al. [23] have also measured Cr evaporation from Crofer 22 APU. The evaporation rates reported in that study for the same materials are however significantly lower than both that reported here and in Ref. [8], which could be the result of a lower collection efficiency.

XRD analysis carried out on the samples exposed for 1000 h confirmed the presence of a corundum and spinel phase. Fig. 4 presents mechanically polished cross sections of the samples that were previously analysed by XRD. The combination of XRD with EDX analysis of the cross sections revealed that the oxide scales consisted of an outer (Cr,Mn)<sub>3</sub>O<sub>4</sub> spinel and inner Cr<sub>2</sub>O<sub>3</sub> corundum layer. EDX analysis also indicated that no Mn remained in the bulk for any of the steels. Further, the quantity of Mn in the spinel appeared to differ for the different steels with those having higher initial Mn contents exhibiting spinels that were richer in Mn. Crofer 22 APU (Fig. 4a) and Crofer 22 H (Fig. 4b) had a Cr:Mn ratio of approximately 1:1 in the spinel, while Sanergy HT (Fig. 4c) and ZMG232 G10 (Fig. 4d) appeared to have Cr:Mn ratios that were closer to 2:1.

Crofer 22 APU formed a 10–12 μm thick oxide with a spinel thickness of 2–4 μm. An internal oxidation zone of Ti-oxide particles was observed below the metal–oxide interface. Crofer 22 H had a total oxide thickness of 9–11 μm and a spinel thickness of 1.5–3 μm. In addition to the Ti oxides below the oxide, Laves phase precipitates were clearly visible along the steel grain boundaries. Sanergy HT (Fig. 4c) had a thinner oxide than Crofer 22 H despite similarities in composition with a total thickness of 6–7 μm and a spinel thickness of 1–2 μm. Fig. 5 presents an EDX line scan through the oxide for Sanergy HT. The scale consists of an inner Cr<sub>2</sub>O<sub>3</sub> layer and an outer Cr–Mn spinel with some Fe enrichment in the spinel layer. What appears as a substantial amount of Mn in the chromia scale is likely a result of the Cr K $\alpha$  X-ray energy



**Fig. 4** – (a–e) SEM-BSE images of the cross section of the steel (a) Crofer 22 APU, (b) Crofer 22 H, (c) Sanergy HT, (d) ZMG232 G10 and (e) E-Brite after exposure in air + 3% H<sub>2</sub>O for 1000 h at 850 °C. The numbered features represent (i) Ni coating used during SEM sample preparation, (ii) (Cr,Mn)<sub>3</sub>O<sub>4</sub> phase, (iii) Cr<sub>2</sub>O<sub>3</sub> phase, (iv) Ti-oxide internal oxidation zone, (v) Laves phase and (vi) Cu enrichment along the metal–oxide interface.

overlapping with the Mn K<sub>β</sub> line. Line scans for the alloys Crofer 22 APU and Crofer 22 H were similar in nature and have been omitted here. The Cu-containing alloy ZMG232 G10 (Fig. 4d), had a thinner oxide that was 4–6 μm thick. No internal oxidation was observed for this alloy which can be attributed to a lack of Ti in the alloy matrix. Fig. 6 shows an EDX line scan through the oxide for this steel. A Cu peak was observed at the metal–oxide interface indicating the enrichment of copper along this boundary. These Cu enrichments are visible as bright spots along the bottom of the oxide scale in Fig. 4d. The oxide scale appeared to be devoid of Cu. This is attributed to the relative thermodynamic stability of Cu compared to the other alloying elements, which prevents it from participating in oxide formation.

After 1000 h of exposure (Fig. 4e) a thin, poorly adherent oxide scale was observed on E-Brite. The oxide scale appeared

to have a porous structure and had a total thickness of 1.5–4 μm. XRD analysis confirmed the presence of a spinel and corundum phase. The poor adherence of the oxide meant that further analysis was difficult using the mechanically polished specimen. An in-situ lift-out was thus produced using a Focused Ion Beam (FIB) and subsequently analysed in the SEM. Fig. 7 presents EDX elemental maps from the lift-out and shows that most of the oxide scale consists of Cr<sub>2</sub>O<sub>3</sub> while some areas on the sample surface are enriched in Mn. These approximately 0.5 μm thick patches are expected to be (Cr,Mn)<sub>3</sub>O<sub>4</sub>. However, in contrast to the other investigated materials, this layer was discontinuous. Furthermore, an enrichment of Si at the metal/oxide interface that forms an almost continuous layer was observed.

#### 4. Discussion

A closer look at the kinetics of oxidation and Cr evaporation reveals the significance of Mn content. The Cr evaporation data in Fig. 3 show a direct relationship between the Mn content of the alloy and its Cr evaporation inhibition properties; higher Mn contents are seen to result in a reduced Cr evaporation rate. This can be evidenced by studying evaporation data for Crofer 22 APU, the steel with the highest Mn content exhibits the lowest Cr evaporation. It is apparent that with decreasing Mn content, the spinel thickness decreases and the Cr evaporation increases. The concentration of Mn in the spinel layer also appears to decrease with decreasing Mn content in the alloy. Thus, the effect of a lower Mn content on the increase in Cr evaporation is attributed to two factors: (1) a thinner spinel layer is less efficient in reducing the supply of Cr, and (2) a lower Mn concentration in the spinel results in higher Cr activity independent of any diffusion reactions. Yasuda et al. [24] claimed that the addition of Cu to the steel ZMG232 G10 lowers Cr evaporation of the material. Such an effect could not be observed in the present study furthermore, considering Fig. 4d and the fact that no Cu is present in the

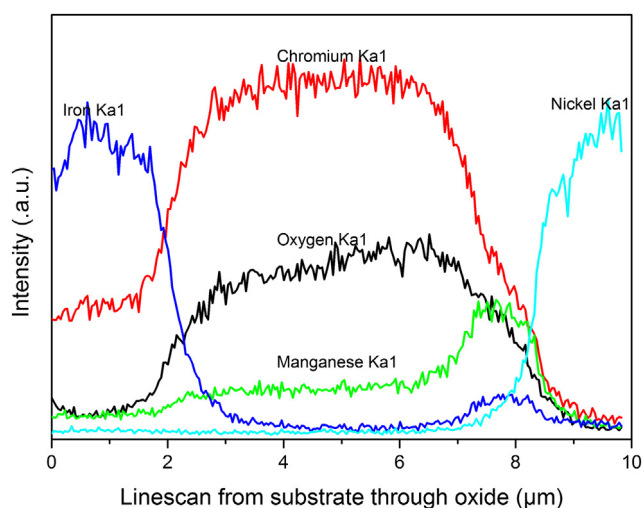


**Fig. 5** – EDX line scan of the oxide formed on Sanergy HT after exposure in air + 3% H<sub>2</sub>O for 1000 h showing the presence of a double layered oxide.

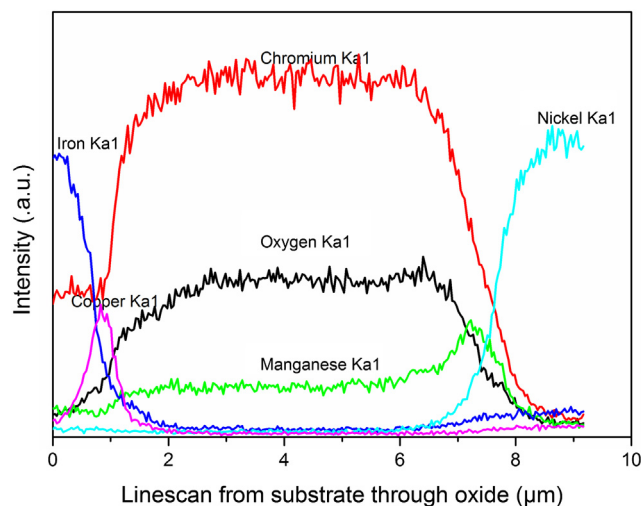


**Fig. 6** – EDX line scan of the oxide formed on ZMG232 G10 after exposure in air + 3% H<sub>2</sub>O for 1000 h showing the presence of a double layered oxide and Cu enrichment at the metal–oxide interface.

oxide scale or on the sample surface, an effect of Cu on Cr evaporation seems unlikely. Furthermore, considering Fig. 4d and the fact that no Cu is present in the oxide scale, an effect of Cu on Cr evaporation seems unlikely. Steels with higher Mn contents also exhibited higher mass gains, which is in line with previous studies such as by Hua et al. [25]. While it is plausible that higher Mn contents will result in a thicker spinel layer and thus a higher mass gain, this only accounts for a part of the difference in oxidation rate. As can be seen in Fig. 4a–e, the chromia scale thickness varies by a factor of 3 for the Fe–22Cr steels. It can be argued that thicker spinels affect the rate of Cr evaporation and thus indirectly the chromia scale thickness. However, the difference in the thickness of the chromia scale is attributed mainly to other factors, such as variations in minor alloying elements. Very small concentrations of rare earth metals are known to play an especially significant role in this respect [26,27].

Furthermore, one should bear in mind that the samples were exposed in as-received state and it is possible that differences in production process or surface treatment can have an effect on the corrosion rate of the material [28].

The weight loss observed for E-Brite is attributed to a combination of Cr evaporation (which is discussed in more detail below) and spallation of the oxide scale. One reason for the poor adhesion of the oxide scale is expected to be the presence of a silica layer beneath the scale (see Fig. 7). Silica has a much lower thermal expansion coefficient than the steel and Cr<sub>2</sub>O<sub>3</sub>, which is considered detrimental for scale adhesion. Another important factor is the lack of reactive elements (RE) in E-Brite; RE additions are known to have a great impact on scale adhesion [26].

Previously reported oxidation data for Sanergy HT supports the findings in this study [29,30]. The testing conditions in those studies vary to some extent but still show comparable oxidation data for Sanergy HT. However, Palcut et al. [17] published fundamentally different oxidation data at 850 °C in air with 1% H<sub>2</sub>O for Sanergy HT, suggesting rapid mass gain and non-parabolic oxidation. This data is unexpected both when considering a Fe–22Cr steel and compared to the more expected results for the Crofer steels in the study by Palcut, which are also supported by the data presented here.

With the available Cr evaporation data it is possible to calculate the mass loss due to Cr evaporation, and subsequently correct the mass gain data for this material loss. Equation (1) allows us to associate the loss of Cr<sub>2</sub>O<sub>3</sub> from the scale to the volatilization of Cr via the formation of CrO<sub>2</sub>(OH)<sub>2</sub>. Thus, every mg of Cr lost from the oxide scale results in an equivalent loss of 1.46 mg of Cr<sub>2</sub>O<sub>3</sub>. Given the linearity of the Cr evaporation process over time, it seems reasonable that an estimate of the mass loss due to Cr evaporation after 1000 h can be made by doubling the value obtained experimentally after 500 h.

Fig. 8 presents the Cr evaporation corrected mass gain curves for the studied steels over 1000 h. The dashed lines in Fig. 8 represent the gravimetrically measured mass gains for the two extreme cases: E-Brite and Crofer 22 APU. It was observed in the case of E-Brite that the apparent negative mass ‘gain’ was due in large part to Cr evaporation. The Cr evaporation corrected mass gain after 1000 h was estimated to

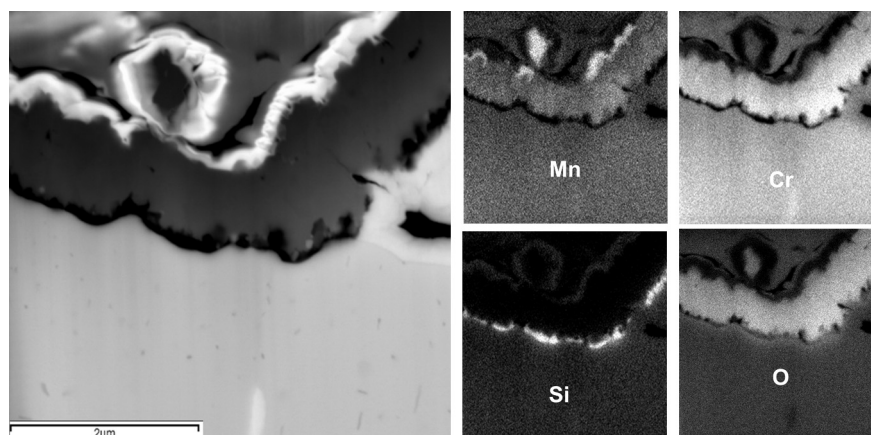


**Fig. 7** – EDX elemental maps for the alloy E-Brite after exposure for 1000 h at 850 °C in air + 3% H<sub>2</sub>O showing a discontinuous spinel layer.

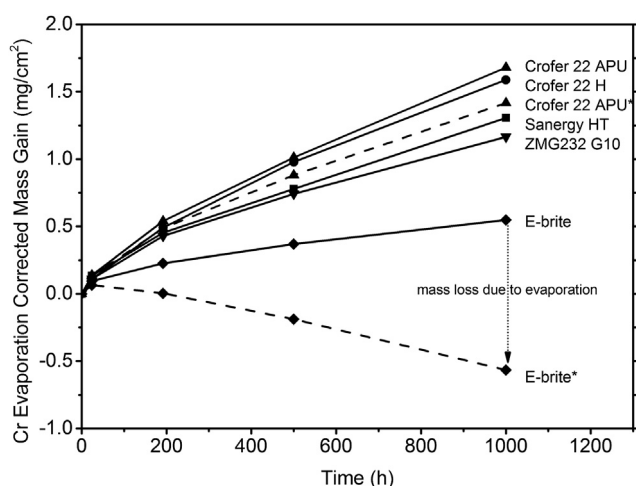


**Fig. 8 – Cr corrected mass gain at 850 °C in air + 3% H<sub>2</sub>O for the analysed steels. The dashed lines represent uncorrected mass gain as measured by gravimetry only for the steels Crofer 22 APU and E-Brite. These lines are marked by an asterisk (\*) in the legend.**

be +0.55 mg/cm<sup>2</sup> instead of –0.56 mg/cm<sup>2</sup>; a difference of 1 mg/cm<sup>2</sup>. The difference between corrected and uncorrected mass gain for Crofer 22 APU is only 0.25 mg/cm<sup>2</sup>. This further demonstrates the effect of the Cr–Mn spinel on Cr evaporation behaviour. A comparison of Figs. 2 and 8 illustrates the limited applicability of mass gain data in estimating interconnect lifetimes or in any other application where Cr volatilization occurs to a significant extent. Furthermore, this comparison elucidates the fact that exposures in stagnant or low flow rate atmospheres could result in misleading experimental data due to the suppression of Cr evaporation if the atmosphere is saturated in Cr<sub>2</sub>(OH)<sub>2</sub>.

Although Cr evaporation was affected by the alloy composition to some extent, it is evident that none of the materials tested in this study are suitable to be used in SOFCs without a protective coating that prevents Cr evaporation.

## 5. Conclusion

The commercial interconnect materials Crofer 22 APU, Crofer 22 H, Sanergy HT, ZMG232 G10 and E-Brite were exposed at 850 °C in a typical SOFC cathode side environment (air + 3% H<sub>2</sub>O). All the investigated steels formed an outer (Cr,Mn)<sub>3</sub>O<sub>4</sub> spinel and inner Cr<sub>2</sub>O<sub>3</sub> corundum layer. However, the spinel layer formed on the steel E-Brite was discontinuous in nature. It was observed that a higher Mn content in the steel led to a lower Cr evaporation rate. Higher Mn contents in a steel result in a thicker and more Mn-rich spinel layer. Both factors are believed to influence Cr evaporation. The steel E-Brite did not contain sufficient Mn to form a continuous outer spinel layer which resulted in a Cr volatilization rate that was approximately four times higher than for the other steels. In the present study, the gravimetric data showed that higher Mn contents resulted in higher mass gains. This is in part due to the above mentioned thicker spinel layer. It was also observed

that the underlying Cr<sub>2</sub>O<sub>3</sub> layer varied substantially in thickness. A commonly underestimated effect on the gravimetric data is the mass loss due to Cr volatilization. A comparison between the uncorrected and Cr evaporation corrected mass gain curves clearly shows that Cr evaporation has a substantial effect on mass gain. Thus, predicting steel lifetimes from mass gain data alone would lead to an overestimation of the useful life of the steel.

## Acknowledgements

The authors would like to thank ThyssenKrupp VDM, Sandvik Materials Technology, Hitachi Metals and ATI Allegheny Ludlum for providing the materials. The financial support received from The Swedish Research Council and Swedish Energy Agency (Grant Agreement No. 34140-1), The Swedish High Temperature Corrosion Centre as well as the Nordic NaCoSOFC project is gratefully acknowledged. Furthermore, the research leading to these results has received funding from the European Union's Seventh Framework Programme (FP7/2007-2013) for the Fuel Cells and Hydrogen Joint Technology Initiative under grant agreement n°[278257].

## REFERENCES

- [1] Brett DJL, Atkinson A, Brandon NP, Skinner SJ. Intermediate temperature solid oxide fuel cells. *Chem Soc Rev* 2008;37:1568–78.
- [2] Kornely M, Neumann A, Menzler NH, Leonide A, Weber A, Ivers-Tiffée E. Degradation of anode supported cell (ASC) performance by Cr-poisoning. *J Power Sources* 2011;196:7203–8.
- [3] Opila EJ, Myers DL, Jacobson NS, Nielsen IMB, Johnson DF, Olminsky JK, et al. Theoretical and experimental investigation of the thermochemistry of Cr<sub>2</sub>(OH)<sub>2</sub>(g). *J Phys Chem A* 2007;111:1971–80.
- [4] Vielstich W, Yokokawa H, Gasteiger HA. Handbook of fuel cells: vol. 5, Advances in electrocatalysis, materials, diagnostics and durability, P. 1/fundamentals, technology and applications. Oxford: Wiley-Blackwell; 2009.
- [5] Jiang SP, Zhen Y. Mechanism of Cr deposition and its application in the development of Cr-tolerant cathodes of solid oxide fuel cells. *Solid State Ionics* 2008;179:1459–64.
- [6] Stanislawski M, Froitzheim J, Niewolak L, Quadackers WJ, Hilpert K, Markus T, et al. Reduction of chromium vaporization from SOFC interconnectors by highly effective coatings. *J Power Sources* 2007;164:578–89.
- [7] Froitzheim J, Canovic S, Nikumaa M, Sachitanand R, Johansson LG, Svensson JE. Long term study of Cr evaporation and high temperature corrosion behaviour of Co coated ferritic steel for solid oxide fuel cell interconnects. *J Power Sources* 2012;220:217–27.
- [8] Stanislawski M, Wessel E, Hilpert K, Markus T, Singheiser L. Chromium vaporization from high-temperature alloys I. Chromia-forming steels and the influence of outer oxide layers. *J Electrochem Soc* 2007;154:A295–306.
- [9] Froitzheim J, Svensson JE. Multifunctional nano-coatings for SOFC interconnects. In: 12th International symposium on solid oxide fuel cells (SOFC) Montreal, Canada Date: May 01–06, 2011. Montreal, Canada.
- [10] Piccardo P, Gannon P, Chevalier S, Viviani M, Barbucci A, Caboche G, et al. ASR evaluation of different kinds of

- coatings on a ferritic stainless steel as SOFC interconnects. *Surf Coat Technol* 2007;202:1221–5.
- [11] Ebrahimifar H, Zandrahimi M. Oxidation and electrical behavior of AISI 430 coated with cobalt spinels for SOFC interconnect applications. *Surf Coat Technol* 2011;206:75–81.
- [12] Macauley C, Gannon P, Deibert M, White P. The influence of pre-treatment on the oxidation behavior of Co coated SOFC interconnects. *Int J Hydrogen Energy* 2011;36:4540–8.
- [13] Choi JP, Weil KS, Chou YM, Stevenson JW, Yang ZG. Development of MnCoO coating with new aluminizing process for planar SOFC stacks. *Int J Hydrogen Energy* 2011;36:4549–56.
- [14] Tondo E, Boniardi M, Cannoletta D, De Riccardis MF, Bozzini B. Electrodeposition of yttria/cobalt oxide and yttria/gold coatings onto ferritic stainless steel for SOFC interconnects. *J Power Sources* 2010;195:4772–8.
- [15] Canovic S, Froitzheim J, Sachitanand R, Nikumaa M, Halvarsson M, Johansson LG, et al. Oxidation of Co- and Ce-nanocoated FeCr steels: a microstructural investigation. *Surf Coat Technol* 2013;215:62–74.
- [16] Froitzheim J, Meier GH, Niewolak L, Ennis PJ, Hattendorf H, Singheiser L, et al. Development of high strength ferritic steel for interconnect application in SOFCs. *J Power Sources* 2008;178:163–73.
- [17] Palcut M, Mikkelsen L, Neufeld K, Chen M, Knibbe R, Hendriksen PV. Corrosion stability of ferritic stainless steels for solid oxide electrolyser cell interconnects. *Corr Sci* 2010;52:3309–20.
- [18] Froitzheim J, Ravash H, Larsson E, Johansson LG, Svensson JE. Investigation of chromium volatilization from FeCr interconnects by a denuder technique. *J Electrochem Soc* 2010;157:B1295–300.
- [19] Seo HS, Yun DW, Kim KY. Oxidation behavior of ferritic stainless steel containing Nb, Nb–Si and Nb–Ti for SOFC interconnect. *Int J Hydrogen Energy* 2013;38:2432–42.
- [20] Froitzheim JH. Ferritic steel interconnectors and their interactions with Ni base anodes in solid oxide fuel cells (SOFC) [Dissertation]. RWTH Aachen; 2008.
- [21] Kuhn B, Jimenez CA, Niewolak L, Hüttel T, Beck T, Hattendorf H, et al. Effect of Laves phase strengthening on the mechanical properties of high Cr ferritic steels for solid oxide fuel cell interconnect application. *Mater Sci Eng A* 2011;528:5888–99.
- [22] Asensio-Jimenez C, Niewolak L, Hattendorf H, Kuhn B, Huczukowski P, Singheiser L, et al. Effect of specimen thickness on the oxidation rate of high chromium ferritic steels: the significance of intrinsic alloy creep strength. *Oxid Metals* 2013;79:15–28.
- [23] Casteel M, Lewis D, Willson P, Alinger M. Ionic conductivity method for measuring vaporized chromium species from solid oxide fuel cell interconnects. *Int J Hydrogen Energy* 2012;37:6818–29.
- [24] Yasuda N, Uehara T, Okamoto M, Yamamura J. Development of a new ferritic alloy for SOFC interconnects with excellent oxidation resistance and reduced Cr-evaporation. Lucerne: European Fuel Cell Forum; 2010.
- [25] Hua B, Kong Y, Zhang W, Pu J, Chi B, Jian L. The effect of Mn on the oxidation behavior and electrical conductivity of Fe-17Cr alloys in solid oxide fuel cell cathode atmosphere. *J Power Sources* 2011;196:7627–38.
- [26] Hou PY, Stringer J. The effect of reactive element additions on the selective oxidation, growth and adhesion of chromia scales. *Mater Sci Eng A* 1995;202:1–10.
- [27] Alman DE, Jablonski PD. Effect of minor elements and a Ce surface treatment on the oxidation behavior of an Fe–22Cr–0.5Mn (Crofer 22 APU) ferritic stainless steel. *Int J Hydrogen Energy* 2007;32:3743–53.
- [28] Niewolak L, Wessel E, Singheiser L, Quadackers WJ. Potential suitability of ferritic and austenitic steels as interconnect materials for solid oxide fuel cells operating at 600 degrees C. *J Power Sources* 2010;195:7600–8.
- [29] Bexell U, Schuisky M, Olsson M. Scratch testing as a tool to evaluate the adhesion of thermally grown oxides on ferritic interconnect steel. Lucerne: European Fuel Cell Forum; 2010.
- [30] Mikkelsen L, Linderroth S, Bilde-Sorensen J. The effect of silicon addition on the high temperature oxidation of a Fe–Cr alloy. *Mater Sci Forum* 2004;461–464:117–22.